Article

Numerical Study of Periodic Magnetic Field Effect on 3D Natural Convection of MWCNT-Water/Nanofluid with Consideration of Aggregation

Lioua Kolsi [2,3,*] , **Hakan F. Oztop [4,9]** , **Kaouther Ghachem [1,3]** , **Mohammed A. Almeshaal [5]** ,
Hussein A. Mohammed [6,*] , **Houman Babazadeh [7,8] and Nidal Abu-Hamdeh [9]**

[1]   Department of Industrial Engineering and Systems, College of Engineering, Princess Nourah Bint
     Abdulrahman University, Riyadh 84428, Saudi Arabia; kgmaatki@pnu.edu.sa
[2]   Department of Mechanical Engineering, College of Engineering, University of Ha'il, Ha'il City 2240,
     Saudi Arabia
[3]   Laboratory of Metrology and Energy systems, Department of Energy Engineering, University of Monastir,
     Monastir 5000, Tunisia
[4]   Department of Mechanical Engineering, Technology Faculty, Firat University, 23119 Elazig, Turkey;
     hfoztop1@gmail.com
[5]   Department of Mechanical Engineering, College of Engineering, Al Imam Mohammad Ibn Saud Islamic
     University, Riyadh 11432, Saudi Arabia; maalmeshaal@imamu.edu.sa
[6]   School of Engineering, Edith Cowan University, 270 Joondalup Drive, Joondalup, WA 6027, Australia
[7]   Department for Management of Science and Technology Development, Ton Duc Thang University,
     Ho Chi Minh City 700000, Vietnam; houman.babazadeh@tdtu.edu.vn
[8]   Faculty of Environment and Labour Safety, Ton Duc Thang University, Ho Chi Minh City 700000, Vietnam
[9]   Department of Mechanical Engineering, King Abdulaziz University, Jeddah 21511, Saudi Arabia;
     nabuhamdeh@kau.edu.sa
[*]   Correspondence: l.kolsi@uoh.edu.sa (L.K.);
     hussein.mohammed@ecu.edu.au or hussein.dash@yahoo.com (H.A.M.)

check for
updates

Abstract: In this paper, a numerical study is performed to investigate the effect of a periodic
magnetic field on three-dimensional free convection of MWCNT (Mutli-Walled Carbone
Nanotubes)-water/nanofluid. Time-dependent governing equations are solved using the finite
volume method under unsteady magnetic field oriented in the x-direction for various Hartmann
numbers, oscillation periods, and nanoparticle volume fractions. The aggregation effect is considered
in the evaluation of the MWCNT-water/nanofluid thermophysical properties. It is found that
oscillation period, the magnitude of the magnetic field, and adding nanoparticles have an important
effect on heat transfer, temperature field, and flow structure.

Keywords: periodic magnetic field; MWCNT-nanofluid; 3D natural convection; aggregation

1. Introduction

The control of the fluid flow and heat transfer via the magnetic damping effect can be
an optimisation parameter in thermal and engineering systems such as microscope design, healthcare
devices, biomechanics, and so on [1].

Izadi et al. [2] performed a numerical investigation on nanofluid's free convection inside a porous
medium using the FEM (Finite Element Method). The authors considered the variable magnetic field
and mentioned that, for higher Ra values, the heat transfer reduces considerably owing to the applied
magnetic field. On the basis of the FEM, Hatami et al. [3] analysed the effects of Fe_3O_4 nanoparticles and
the variable magnetic field on natural convection. They mentioned that, owing to the induced Lorentz

force, increasing the Hartman number causes a decrease in heat transfer. Hashim et al. [4] focused on unsteady flow of non-Newtonian Williamson nanofluid under the effect of a variable magnetic field and observed an enhancement of heat transfer rate with the Schmidt number. Sheikholeslami and Vajravelu [5] studied the Fe_3O_4/water flow under constant heat flux using CVFEM (Control Volume Finite Element Method). They concluded that the Rayleigh number and nanoparticles' concentration increase the average temperature.

Sandeep and Animasaun [6] reported a work on the enhancement of heat transfer by adding nanoparticles. They included magnetic field effects. They compared two nanofluids and found that heat transfer rate of water-AA7075/nanofluid is significantly higher than that of water-AA072/nanofluid. Hatami et al. [7] investigated the effects of variable magnetic field on the MHD (Magnetohydrodynamics) forced convection of Al_2O_3–water nanofluid. They considered a porous flat plate with nonlinear stretching. Shah et al. [8] studied the influence of a variable magnetic field on the viscous fluid flow, heat, and mass transfer using analytical and numerical techniques using the homotopy analysis method. They observed that pressure and torque on the discs are highly affected by the distance between discs.

Nimmagadda et al. [9] studied the effect of jet impingement uniform on heat transfer of nanofluid under a non-uniform magnetic field. They found that the enhancement of heat transfer can reach 173% for a volume fraction of 3%. Nassar et al. [10] applied the magnetic field on thermoelectric cooler (TEC) to control working conditions at different magnetic field intensities.

Kefayati [11] used the LBM (Lattice Boltzmann method) technique to simulate the natural convection under sinusoidally varying temperature under a magnetic field. Al-Salem et al. [12] investigate the mixed convection with a driven lid. They observed an important decrease of that transfer with the Hartmann number. Bao et al. [13] applied the non-uniform magnetic field to simulate the heat and mass transfer during evaporation of mixed nitrogen and liquid oxygen. The effects of magnetic field direction on film boiling nanofluid are studied by Malvandi [14]. He indicated that the direction is an important parameter on boiling. Nessab et al. [15] conducted work on ferrofluid jet flow and heat transfer with the presence of a magnetic field. They observed that the heat transfer is increased with the increase of the (Mn) number and reduces with the opening ratio (R). The effects of magnetic field are tested for carbon nanotubes suspensions [16], peristaltic flow of Jeffrey fluid [17], unsteady separated stagnation-point flow [18], and forced convection through semi-annulus [19]. Qin et al. [20] offers a new, simpler approach that, for the first time, makes it possible to continuously measure the reflectivity of non-touchable surfaces. More details about the subject can be found in the literature [21–52].

The main purpose of this paper is to test the application of variable magnetic field on heat transfer and fluid structure in a three-dimensional cavity filled with MWCNT-nanofluid. On the basis of the authors' knowledge and wide literature survey, natural convection in MWCNT-nanofluid filled 3D cavities under periodic magnetic field has not been studied. Thus, the study will help to readers to understand the mechanism of control of heat transfer via variable magnetic field.

2. Physical Model

The considered configuration with boundary conditions is presented on Figure 1. The flow is considered as laminar and tow vertical walls are at a constant temperature (T_h and T_c). The remaining walls are considered adiabatic. A periodic external magnetic field is applied along the x-direction. The cavity is filled with a MWCNT-water nanofluid. The properties of MWCNT and water are presented in Table 1.
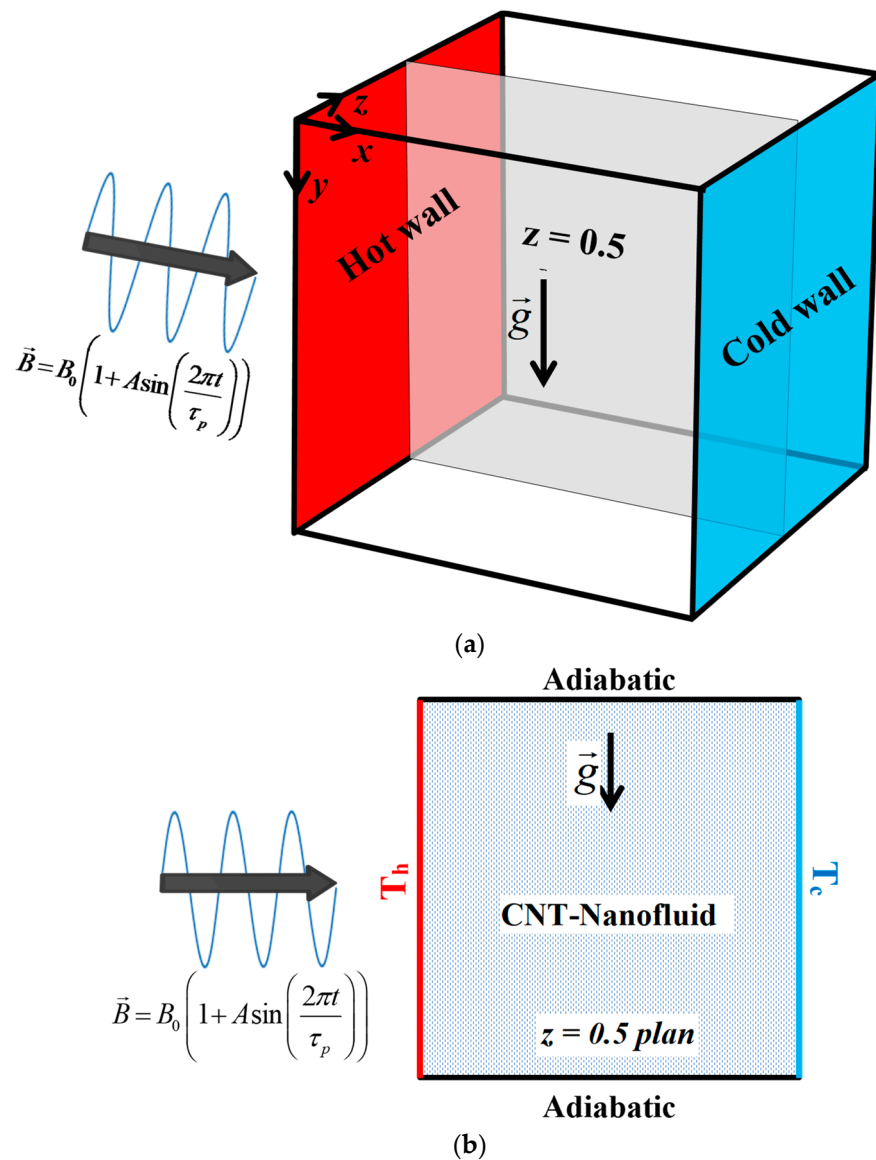
Figure 1. (**a**) Three dimensional configuration; (**b**) z = 0.5 plan with boundary conditions.

2.1. Governing Equations

To simplify the resolution of the governing equations, the 3D vorticity vector potential formalism was used. In fact, it allows the elimination of the pressure gradient terms.

The vorticity and vector potential are expressed as follows:

$$\vec{w}' = \vec{\nabla} \times \vec{U}',$$ (1)

and

$$\vec{U}' = \vec{\nabla} \times \vec{\psi}'.$$ (2)

To get the dimensionless governing equations, the variables Φ', $\vec{B}'$, $\vec{J}'$, $\vec{w}'$, $\vec{\psi}'$, $\vec{V}'$ and t', are divided by $l \cdot v_0 \cdot B_0$, B_0, $\sigma \cdot v_0 \cdot B_0$, l^2/α, α, α/l, and l^2/α, respectively, and $\theta = (T' - T_c')/(T_h' - T_c')$

$$-\vec{w} = \nabla^2 \vec{\psi},$$ (3)

$$\frac{\partial \vec{w}}{\partial t} + (\vec{U} \cdot \nabla)\vec{w} = (\vec{w} \cdot \nabla)\vec{U} + \frac{\nu_{nf}}{\nu_f} \mathrm{Pr} \cdot \nabla^2 \vec{w} - \frac{\beta_{nf}}{\beta_f} Ra \mathrm{Pr} \nabla \times \theta \vec{g}$$

$$+ \frac{\rho_f}{\rho_{nf}} \cdot \frac{\sigma_{nf}}{\sigma_f} Ha^2 \cdot \mathrm{Pr} \cdot \nabla \times \left(\vec{j} \times \vec{e}_B \right) \tag{4}$$

$$\frac{\partial \theta}{\partial t} + \vec{U} \cdot \nabla \theta = \frac{\alpha_{nf}}{\alpha_f} \nabla^2 \theta, \tag{5}$$

$$\vec{j} = -\vec{\nabla}\Phi + \vec{U} \times \vec{e}_B, \tag{6}$$

$$\vec{\nabla}^2 \Phi = \vec{\nabla} \cdot (\vec{U} \times \vec{B}) = -\vec{e}_B \cdot \vec{w}, \tag{7}$$

with

$$\vec{B} = B_0 \left(1 + A \sin\left(\frac{2\pi t}{\tau_p} \right) \right), \tag{8}$$

with

$$\mathrm{Pr} = \frac{\nu_f}{\alpha_f}, \; Ra = \frac{g \cdot \beta_f \cdot \Delta T \cdot l^3}{\nu_f \cdot \alpha_f}, \; \text{and } Ha = B_0 l \sqrt{\frac{\sigma_f}{\rho_f \nu_f}}. \tag{9}$$

The effective thermophysical properties are evaluated using the following expressions:

- Density:

$$\rho_{nf} = \rho_f (1 - \varphi) + \rho_s \varphi. \tag{10}$$

- Heat capacitance:

$$\left(\rho C_p \right)_{nf} = \varphi \left(\rho C_p \right)_s + (1 - \varphi) \left(\rho C_p \right)_f. \tag{11}$$

- Dynamic viscosity:

Taking into account the fractal shape of aggregates [25], the modified nanoparticle volume fraction (volume fraction of the aggregates in water), ϕ_{ag}, is expressed as follows:

$$\phi_{ag} = \phi \left(\frac{r_a}{r_p} \right)^{3-D}, \tag{12}$$

where

- r_a is the radii of the aggregates;
- r_p is the radii of the primary solid particles;
- D is the fractal index depending on shear flow condition and type, size, and shape of the aggregates.

Thus, based on the Maron and Pierce model [26] and the expression of the modified volume fraction, the effective viscosity of the MWCNT-nanofluid can be expressed as follows:

$$\frac{\mu_{nf}}{\mu_f} = \left(1 - \frac{\phi \left(\frac{r_a}{r_p} \right)^{3-D}}{\phi_m} \right)^{-2}. \tag{13}$$

On the basis of the experimental work of Halelfadl et al. [27] for MWCNT with $l_p = 1.5$ µm and $d_p = 9.2$ nm, it was determined that $D = 2.1$, $\phi_m = 0.0361$, and $r_a/r_p = 4.41$.

- Thermal conductivity (Xue-model):

On the basis of Nan's model [28] and taking into account the aggregates effect, the effective thermal conductivity of MWCNT is calculated using the following expressions:

$$\frac{\lambda_{nf}}{\lambda_f} = \frac{3 + \phi_{\text{int}}(\beta_{11} - \beta_{33})}{3 - \phi\beta_{11}},$$

$$\beta_{11} = \frac{\lambda_{11} - \lambda_f}{\lambda_f + 0.5(\lambda_s - \lambda_f)}, \ \beta_{33} = \frac{\lambda_{33}}{\lambda_f} - 1, \ \lambda_{11} = \frac{\lambda_s}{1 + \frac{2a_k}{d_p}\frac{\lambda_s}{\lambda_f}}, \ \lambda_{33} = -\frac{\lambda_s}{1 + \frac{2a_k}{l_p}\frac{\lambda_s}{\lambda_f}}, \ a_k = R_k \cdot \lambda_f \quad (14)$$

where

- λ_{11} is the transverse thermal conductivity;
- λ_{33} is the longitudinal thermal conductivity;
- d_p is the nanoparticle diameter;
- l_p is the nanoparticle length;
- a_k is the Kapitza radius;
- R_k is the Kapitza resistance (fixed at $8.83 \times 10^{-8} \text{m}^2 \text{ K/W}$);
- $\phi_{\text{int}} = \frac{\phi}{\phi_{ag}}$ is volume fraction of the MWCNT in the aggregate.

- electrical conductivity:

$$\sigma_{nf} = \sigma_f \left[1 + \frac{3 \cdot \varphi \cdot \left(\frac{\sigma_s}{\sigma_f} - 1 \right)}{\left(\frac{\sigma_s}{\sigma_f} + 2 \right) - \varphi \cdot \left(\frac{\sigma_s}{\sigma_f} - 1 \right)} \right] \quad (15)$$

The local and average Nusselt numbers are evaluated using the following:

$$Nu = \left(\frac{\lambda_{nf}}{\lambda_f} \right) \frac{\partial \theta}{\partial x} \bigg|_{x=0} \text{ and } Nu_{av} = \int_0^1 \int_0^1 Nu \cdot dy \cdot dz \quad (16)$$

As the applied magnetic field in this study is periodic, it is expected that Nu_{av} will be periodic; thus, a time averaged Nusselt number (Nu_{av}^t) is defined as follows:

$$Nu_{av}^t = \int_t^{t+\tau_p} Nu_{av}^t \cdot dt. \quad (17)$$

The solution is considered satisfactory if Equation (18) is satisfied in each time:

$$\sum_i^{1,2,3} \frac{\max|\psi_i^m - \psi_i^{m-1}|}{\max|\psi_i^m|} + \max|T_i^m - T_i^{m-1}| \leq 10^{-5}. \quad (18)$$

2.2. Boundary Conditions

The boundary conditions for the present problem are given as follows:
Temperature:
$\theta = 0$ on the right wall, and $\theta = 1$ on the left wall.
$\frac{\partial \theta}{\partial n} = 0$ on the remaining walls.
Vorticity:
$w_y = -\frac{\partial U_z}{\partial x}, w_x = 0, w_z = \frac{\partial U_y}{\partial x}$ at $x = 0$ and 1.
$w_x = \frac{\partial U_z}{\partial y}, w_y = 0, w_z = \frac{\partial U_x}{\partial y}$ at $y = 0$ and 1.
$w_x = -\frac{\partial U_y}{\partial z}, w_y = \frac{\partial U_x}{\partial z}, w_z = 0$ at $z = 0$ and 1.
Vector potential:
$\frac{\partial \psi_x}{\partial x} = \psi_y = \psi_z = 0$ at $x = 0$ and 1.

$\psi_x = \frac{\partial \psi_y}{\partial y} = \psi_z = 0$ at $y = 0$ and 1.

$\psi_x = \psi_y = \frac{\partial \psi_z}{\partial z} = 0$ at $z = 0$ and 1.

Velocity:

$U_x = U_y = U_z = 0$ on all walls.

Electric potential:

$\frac{\partial \Phi}{\partial n} = 0$ on all walls.

Current density:

$\vec{J} \cdot \vec{n} = 0$ on all walls.

Table 1. Properties of water and MWCNT nanoparticles.

Property	Water	MWCNT
C_p (kJ/kg·K)	4.179	0.796
ρ (kg/m^3)	997.1	1600
λ (kW/m·K)	0.613×10^{-3}	3
β (K^{-1})	21×10^{-5}	4.2×10^{-5}
$\sigma \cdot$ (Ω^{-1}·m^{-1})	5×10^{-2}	4.8×10^{-7}
μ (Pa·s)	0.85×10^{-3}	-

3. Solution Procedure, Grid Sensitivity Test, and Validation

The central-difference scheme based control volume method is used to discretize Governing Equations (4)–(8). The fully implicit procedure and central-difference scheme are used to treat the temporal derivatives and the convective terms, respectively.

The grid independency test was performed for $Ha = 50$, $\varphi = 0.05$, and $\tau_p = 1$. The tests were conducted for different grids. The time averaged Nusselt number was the sensitive parameter. The incremental increase between the grid $81 \times 81 \times 81$ and $91 \times 91 \times 91$ is only 0.333% (Table 2). For solution accuracy and time economy, a spatial mesh size of $81 \times 81 \times 81$ is retained to perform all the simulations.

Table 2. Grid independency test.

Grid	Nu_{av}^t	Increase (%)	Incremental Increase
$61 \times 61 \times 61$	6.0251	-	-
$71 \times 71 \times 71$	6.04579	0.34339679	-
$81 \times 81 \times 81$	6.10967	1.39999981	1.05660302
$91 \times 91 \times 91$	6.13002	1.73307836	0.33307855

The verification of the present code is firstly performed by comparing with results Okada and Ozoe [29], who proposed an experimental correlation (Equation (19)) allowing the evaluation of the Nusselt number as function of the Hartman and Grashof numbers for the case of gallium filled cubical cavity. Figure 2 shows an excellent concordance with the results of Okada and Ozoe [29].

$$\frac{Nu_B - 1}{Nu_0 - 1} = 1 - \left[1 + \left(0.57 \cdot Gr^{1/3}/Ha\right)^{3.19}\right]^{-1/1.76} \tag{19}$$
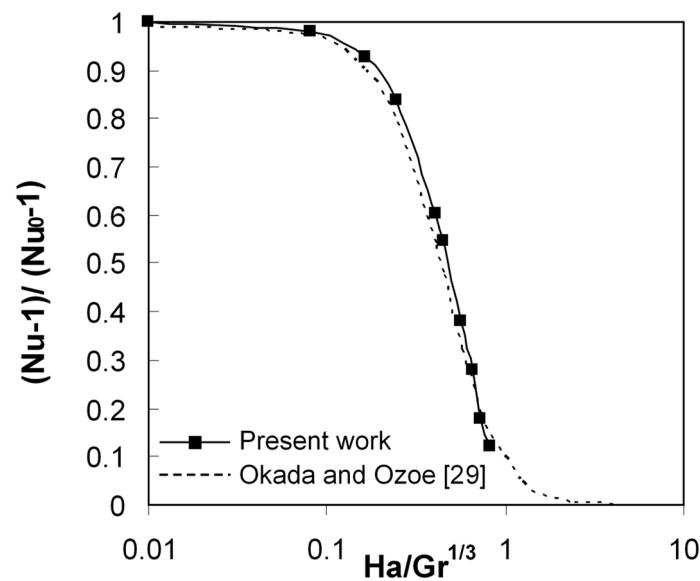
Figure 2. Comparison with the results of Okada and Ozoe [29].

In the case of nanofluids, a comparison was performed with the results of Jahanshahi et al. [30]. As presented in Figure 3, the comparison also shows a good agreement.
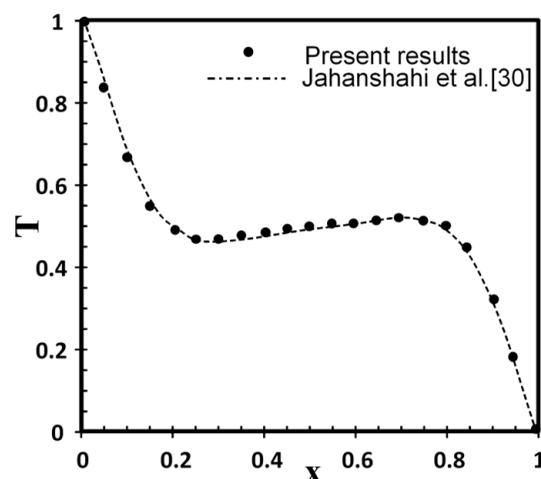

Figure 3. Comparison with the results of Jahanshahi et al. [30].

4. Results and Discussion

A finite volume based computational work was performed to investigate the three-dimensional natural convection of MWCNT-water/nanofluid filled cavity under variable magnetic field. While adding MWCNT particles enhances the heat transfer owing to high effective thermal conductivity, the application of a magnetic field opposes this enhancement. Thus, the simultaneous influence of a variable magnetic field and adding nanoparticles on the 3D flow and heat transfer is investigated.

The periodic magnetic field is considered along the x-direction. The Rayleigh number is fixed at $Ra = 10^5$ and the amplitude (A) is fixed at 0.5, so that the magnitude of the magnetic field oscillates between $0.5B_0$ and $1.5B_0$. Owing to the relatively low considered volume fractions, the single phase model is adopted. The ranges of Hartman number, MWCNT volume fraction, and oscillation period are ($0 \leq Ha \leq 100$), ($0 \leq \varphi \leq 0.05$), and ($0.01 \leq \tau_p \leq 10$), respectively.

In absence of a magnetic forces, the flow structure and temperature field are presented in Figure 4. The flow structure is shown via some particle trajectories. For $\varphi = 0$ (pure water), two central clockwise vortices characterize the flow structure. Adding MWCNT particles was found to enhance the buoyancy

forces and to increase the size of the vortices. The particle paths are shifted towards the isothermal walls and the vortices become adjacent to these walls.

It is to be noted that the maximum of the velocity magnitude is lowered by adding nanoparticles owing to the inter-particular friction caused by the increase of the viscosity. The maximal values of the magnitude of the velocity are located near to the active walls because of the important gradients of temperatures in these regions.

Figure 4c presents the temperature field for Ha = 0. The iso-surfaces of temperature are vertically stratified at the core region and distorted near of the active walls. This phenomenon becomes more pronounced by adding the MWCNT nanoparticles with an increase of the temperature gradient.
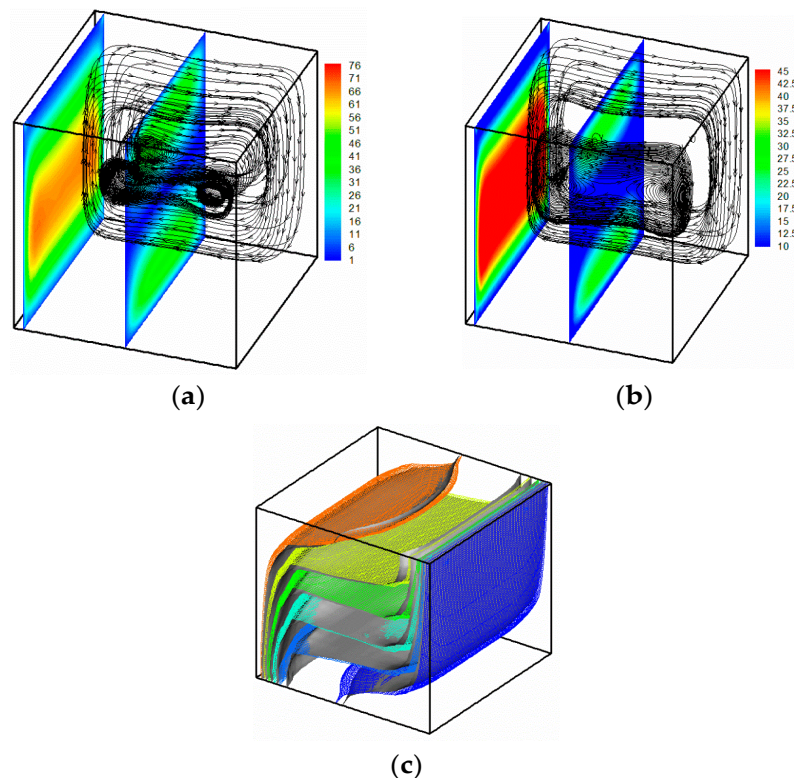
(a)

(b)

(c)

Figure 4. Flow structure (**a**): φ = 0 and (**b**) φ = 0.05 and temperature field (**c**): φ = 0.05 (coloured) and φ = 0 (grey).

Figure 5 presents the 3D pathlines and velocity magnitude at different times of the oscillation period for Ha = 50 and τ_p = 1. The results for pure water are presented on the left side and those of MWCNT-water nanofluid with φ = 0.05 are presented on the right. The interaction between the magnetic field and the fluid motion generates a Lorentz force that opposes the buoyancy forces, causing the damping effect. This damping is more important near the active walls, except near the corners. In fact, because of the electric insulation of the walls, the electric current is redirected, and thus the Lorentz force vanishes in these regions. In addition, a merging phenomenon occurs and the pathlines become characterized by only one clockwise vortex.
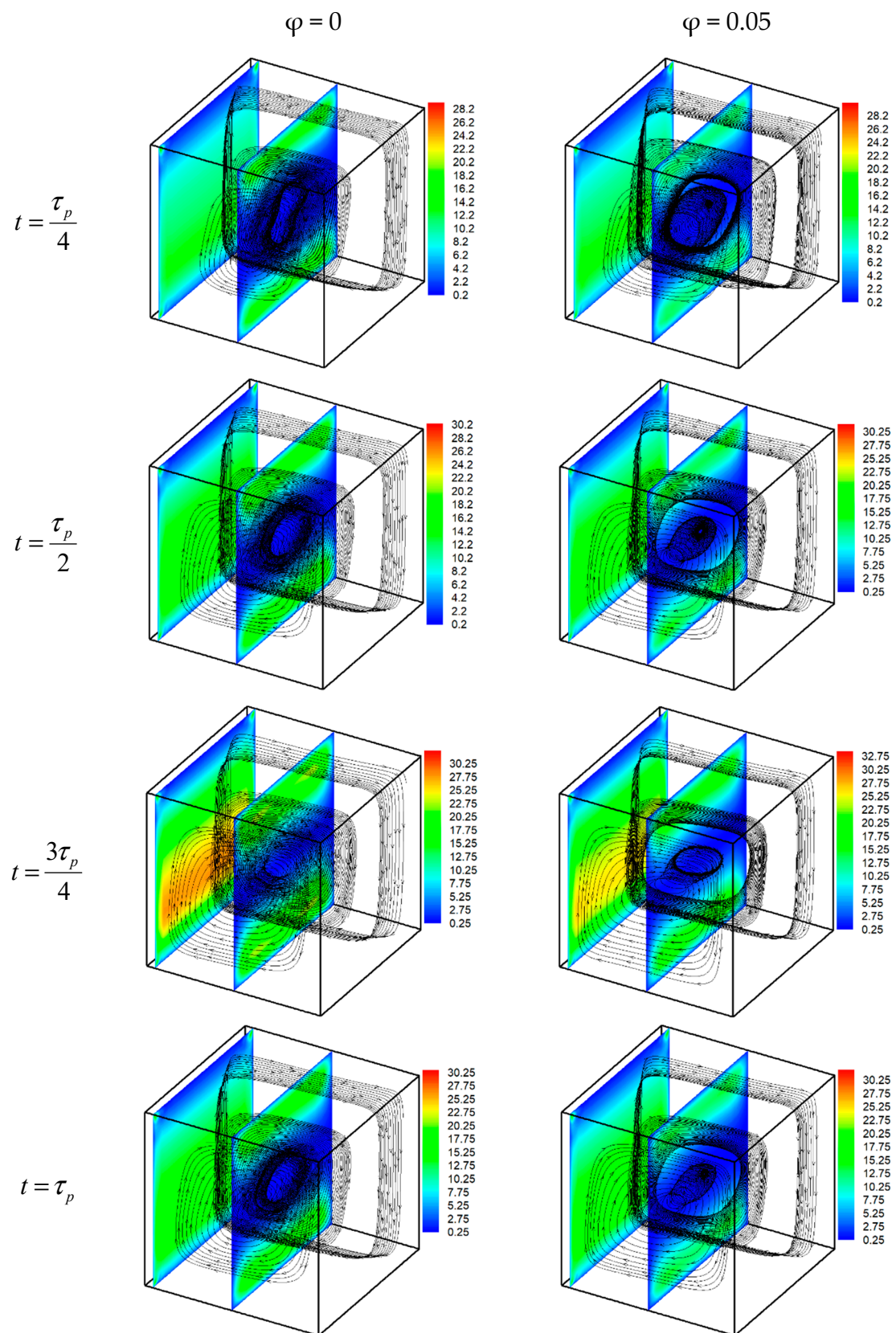
$\varphi = 0$　　　　　　　　　　　　$\varphi = 0.05$

$t = \dfrac{\tau_p}{4}$

$t = \dfrac{\tau_p}{2}$

$t = \dfrac{3\tau_p}{4}$

$t = \tau_p$

Figure 5. Pathlines and velocity magnitude for Ha = 50 and $\tau_p = 1$.

The lateral flow (near of the walls) is also affected by the applied magnetic field and the longitudinal flow becomes less pronounced owing to the reduction of the 3D character (MHD bi-dimensionalization). The structure and the intensity of the flow change slightly during the oscillation period. In fact, the size and the shape of the vortexes change periodically with the time.

Figure 6 shows the velocity vectors projection at z = 0.5 plan for φ = 0.05, Ha = 25, and A = 0.5 at different times and different oscillation periods. Owing to the magnetic effect, there is a change from a roll structure to a square structure; this conclusion was also mentioned by Al-Najem et al. [31]. It is seen that, for all chosen oscillation periods, the main flow structure changes periodically with time. In fact, vortexes' merging and division occur during the period for all considered τ_p values. Thus, owing to the periodic magnitude of the magnetic field, the flow structure oscillates between one and two central vortexes. In addition to the number of vortexes, their shape also changes with time.

As presented in Figure 7, for higher Hartman numbers (Ha = 100), the merging-division phenomenon persists, but with a flow structure having a slope that approaches the vertical. The flows near the active walls are more attenuated owing to the magnetic damping. This result is also recalled by Ozoe and Okada [29], by mentioning that the induced Lorentz force opposes the flow perpendicular to the direction of the magnetic field. In fact, compared with the Ha = 25 case, in which the maximum values of velocity magnitude are near of the active walls, for Ha = 100, the maximums become near to the top and bottom walls. In opposition with all other τ_p values, for $\tau_p = 0.01$ when the merging occurs at $t = \frac{\tau_p}{2}$, the central symmetry disappears, in fact, the vortex is located in the highest region of the enclosure.

Figure 8 presents a sequence of the temperature field for different Hartmann numbers. The vertical stratification described in Figure 4 is reduced by applying the magnetic (Ha = 50) and, for high values of Hartman number (Ha = 100), the stratification disappears completely. Owing to the suppression of the convective forces opposed by the Lorentz force, the temperature field becomes similar to the conductive regime with an important decrease of the temperature gradients near to the active walls. This conclusion is confirmed by the experimental work of Xu et al. [32]. Owing to their high thermal conductivity, the addition of MWCNT nanoparticles opposes the heat transfer diminution caused by the presence of the magnetic field. Thus, the reduction of the vertical stratification is less pronounced for the case of MWCNT-water compared with pure water. Similarly to the flow structure, the temperature field also changes during the period. For a better understanding of this change, the isotherms at the central plan (Figure 9) for $\tau_p = 1$, φ = 0.05, and A = 0.5.

From this figure, it is seen that isotherms are clearly modified with time, especially at the core of the cavity. In fact, near of the active walls, the isotherms are almost similar during the period and different at the core region. It is to be noted that these changes are more pronounced for higher Hartman values owing to the increase of the extremum of the magnitude of the magnetic field.
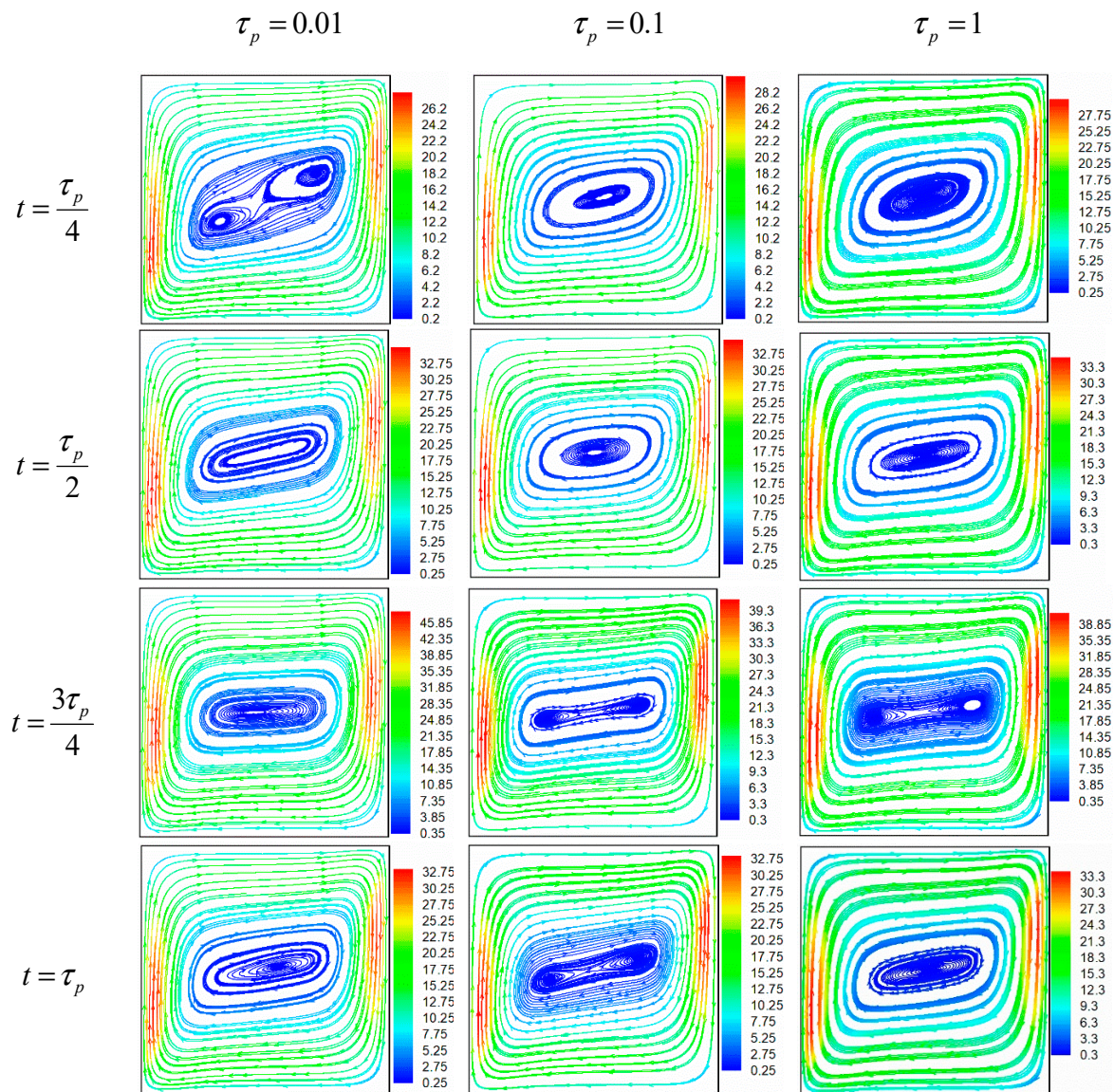
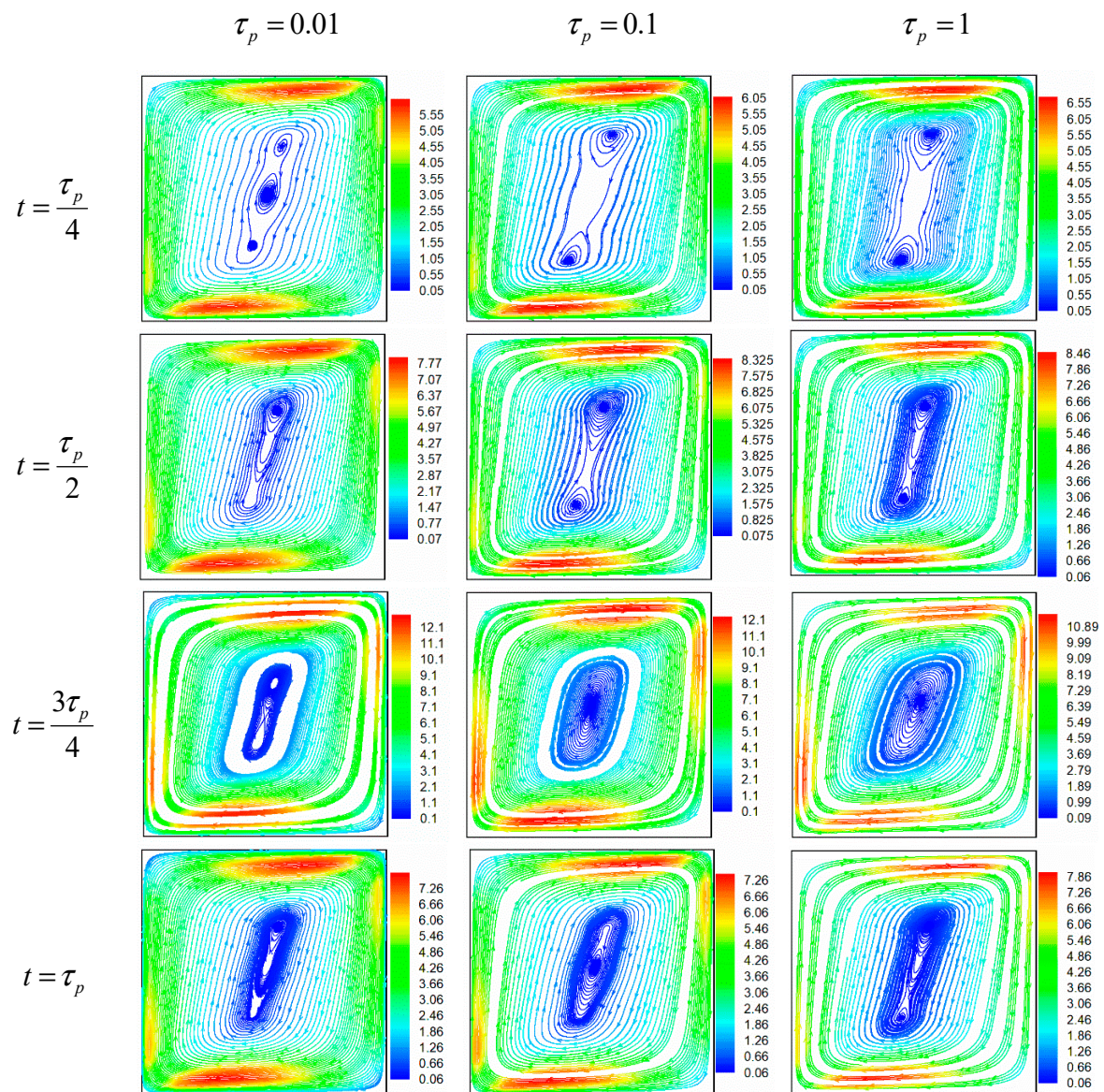**Figure 6.** Streamlines for $\varphi = 0.05$, Ha = 25, and A = 0.5.

$\tau_p = 0.01$ $\tau_p = 0.1$ $\tau_p = 1$

$t = \dfrac{\tau_p}{4}$

$t = \dfrac{\tau_p}{2}$

$t = \dfrac{3\tau_p}{4}$

$t = \tau_p$

Figure 7. Streamlines for $\varphi = 0.05$, Ha = 100, and A = 0.5.

Ha = 50   Ha = 100

$t = \dfrac{\tau_p}{4}$
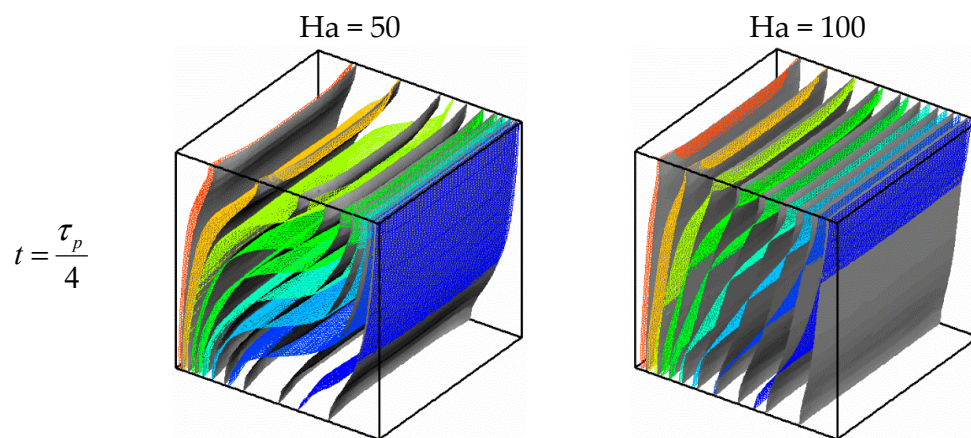
Figure 8. *Cont.*

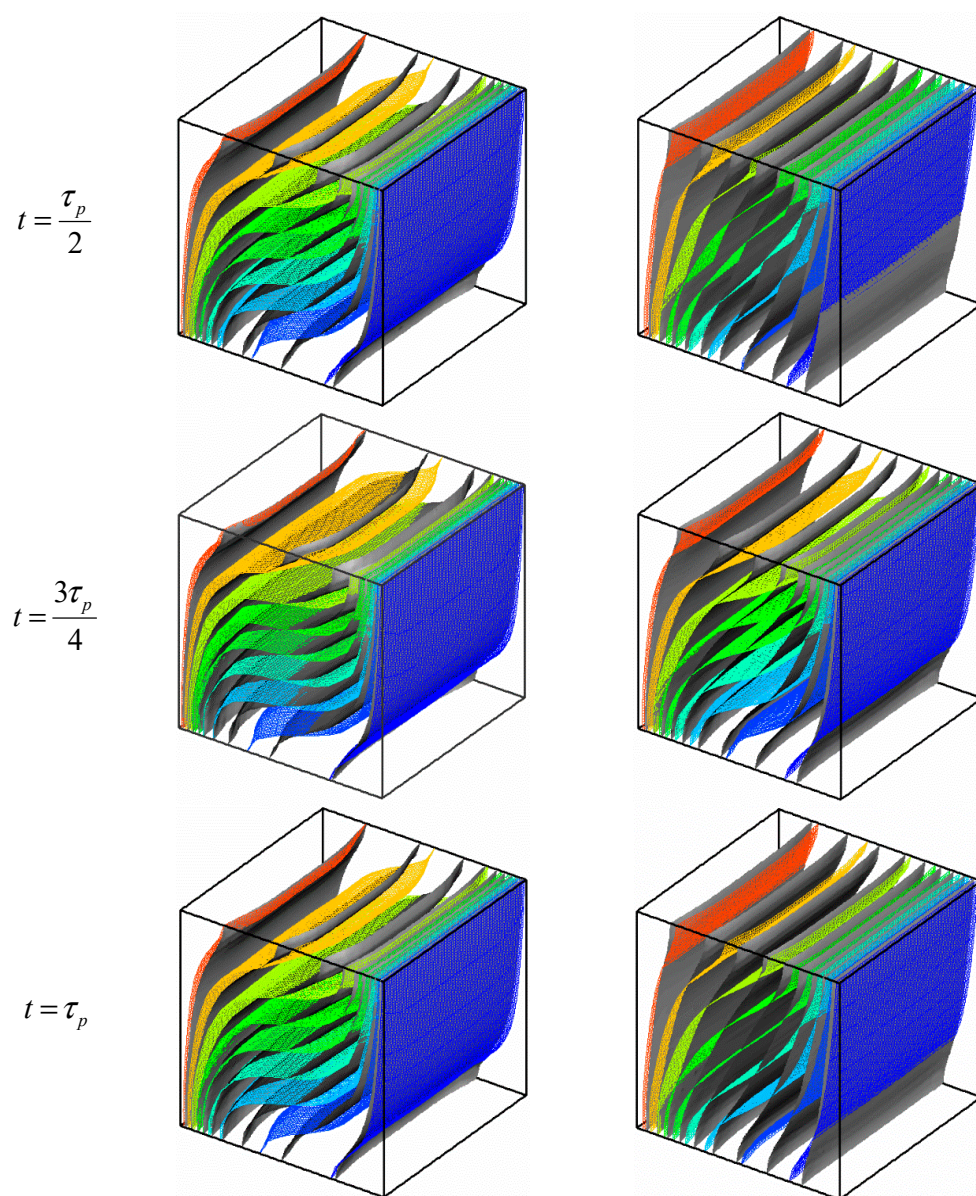**Figure 8.** Isosurfaces of temperature for different Ha and times; φ = 0.05 (multicolour) and φ = 0 (grey).

Figure 10 illustrates the effect of adding nanoparticles on isotherms at the central plan for τ_p = 0.1 and A = 0.5 (flood (φ = 0.05) and line (φ = 0)). As seen from the figure, that addition of nanoparticle to base fluid has an important effect on temperature distribution. Isotherms become steeper with the increasing Ha number. This means that heat transfer turns to conduction mode. As mentioned above, the isotherms' structure varies during the period, especially in the central zones for all Hartman values and nanoparticles concentrations.

Figure 11 presents the effect of the time-periodic magnetic field magnitude on the average Nusselt number at a certain value of Hartman numbers and nanoparticles volume fraction. As the magnetic field is periodic, it is obvious that the results show the fluctuation in amplitude of the average Nusselt number around a certain value. By decreasing the oscillation period (τ_p), the fluctuation decreases, especially for high Hartman values (Figure 11), but it does not become zero. It is to be noted that the average value around which the Nusselt number fluctuates decreases by increasing τ_p; this is an interesting result when the purpose is to reduce the heat transfer. Obviously, the effects of the applied magnetic field and adding nanoparticles are opposite. In fact, the Nusselt number decreases with Ha and increases with φ.
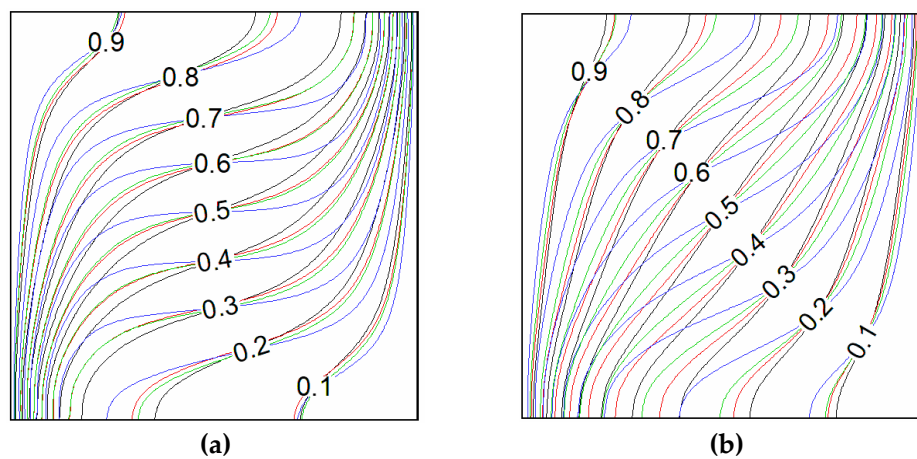
Figure 9. Isotherms for different Ha at $\tau_p = 1$, $\varphi = 0.05$, A = 0.5, black ($\tau_p/4$), red ($\tau_p/2$), blue ($3\,\tau_p/4$), and green (τ_p); (**a**) Ha = 50; (**b**) Ha = 100.
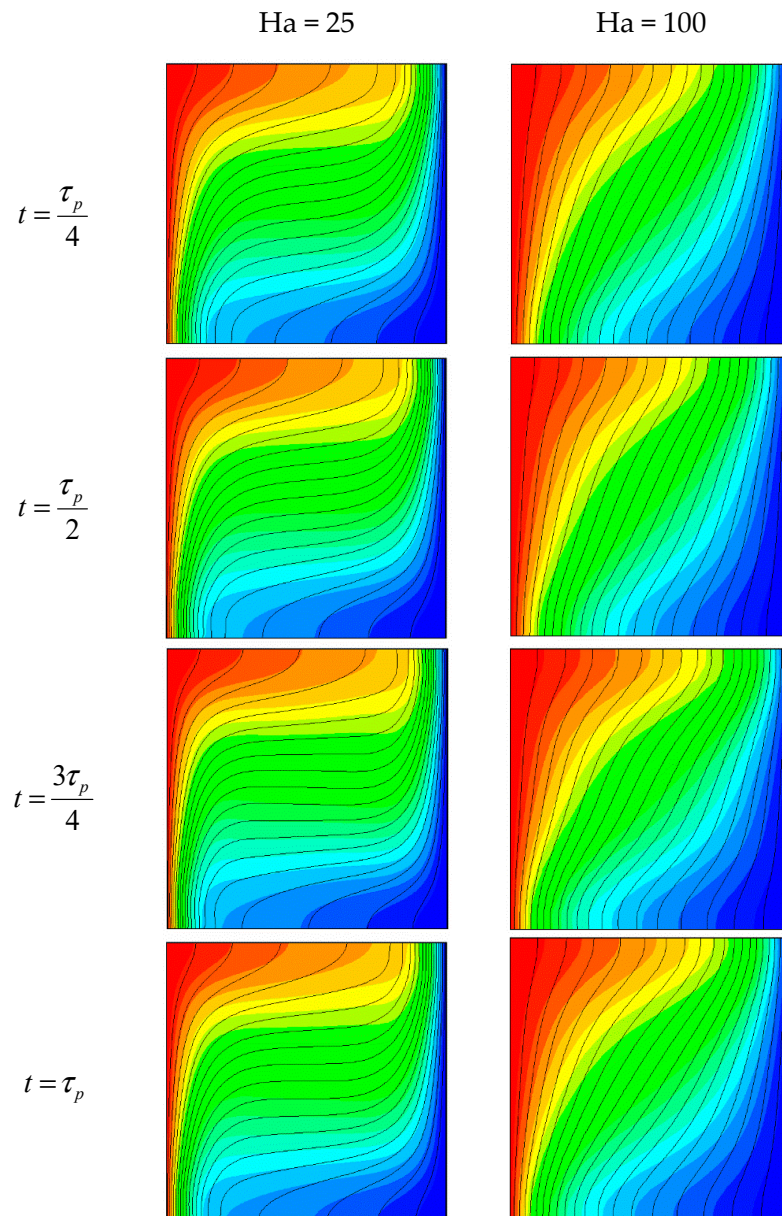

Figure 10. Isotherms for $\tau_p = 0.1$, A = 0.5 flood ($\varphi = 0.05$), and line ($\varphi = 0$).
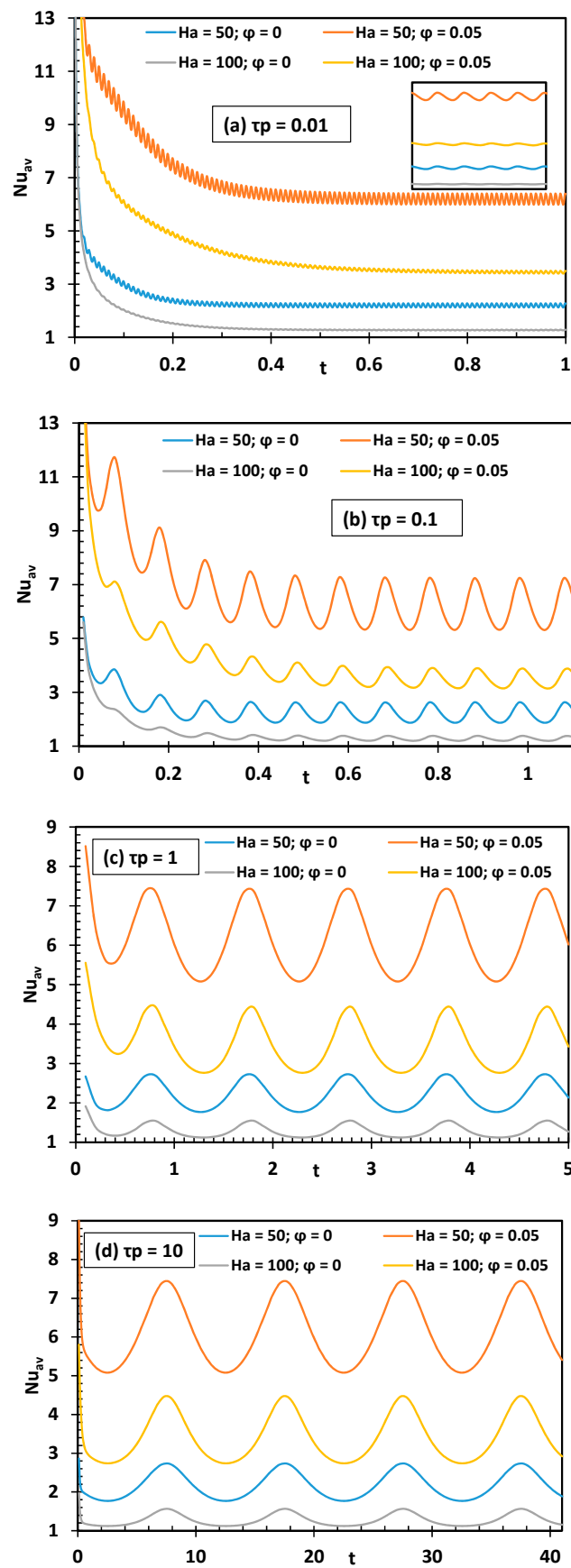
Figure 11. Temporal evolution of the Nusselt number for different magnetic field oscillation period, Hartmann number, and nanoparticle concentration.

Figure 12 illustrates the effect of nanoparticles volume fraction on the time-averaged Nusselt number (Nu_{av}^t) for different Ha and τ_p. Firstly, it is noted that the effect of τ_p on (Nu_{av}^t) is very limited. The applied magnetic field reduces the heat transfer for all values of τ_p and Ha. In opposition, owing to the higher thermal conductivity, increasing nanoparticles volume fraction enhances considerably the heat transfer.
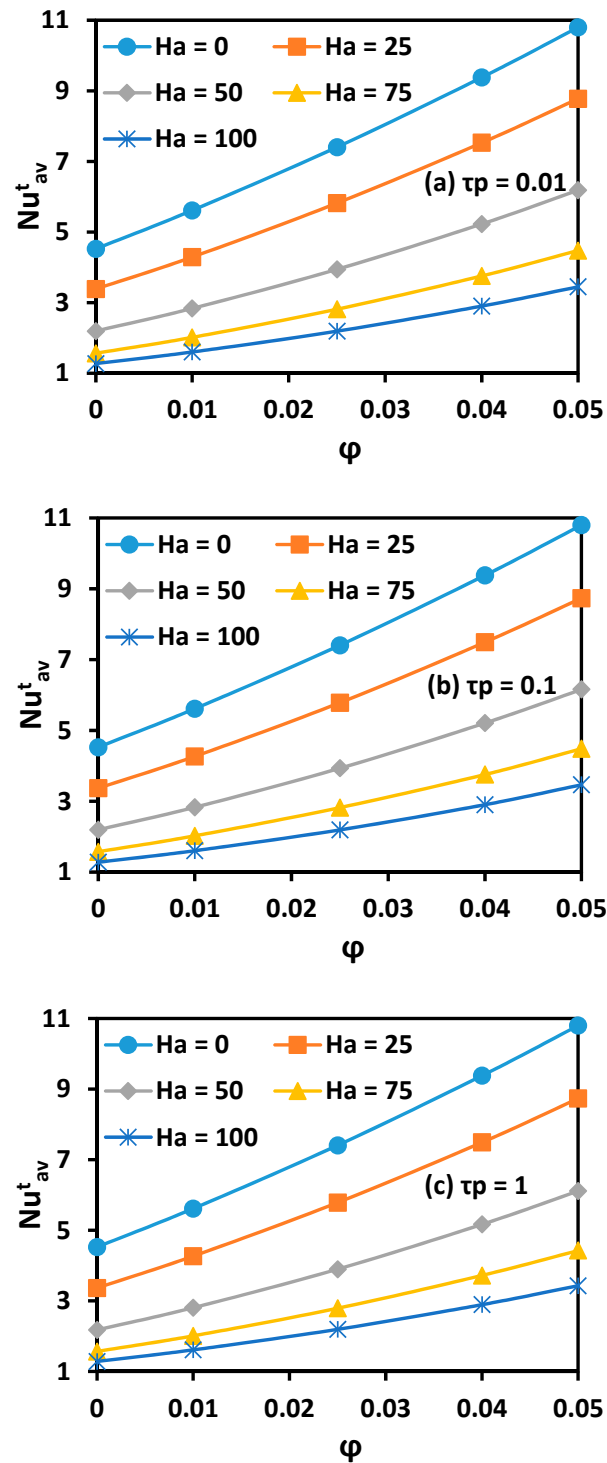

Figure 12. *Cont.*
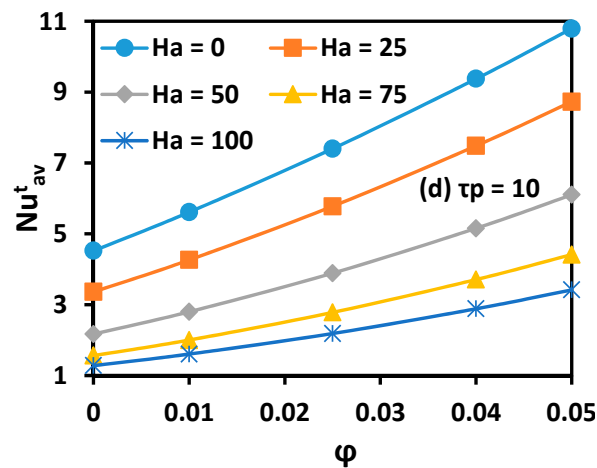
Figure 12. MWCNT volume fraction effect on time averaged Nusselt number (Nu_{av}^t) for different Ha and τ_p.

5. Conclusions

A computational work was conducted on heat transfer and fluid flow inside a three-dimensional closed space under a variable magnetic field. The main findings are as follows:

- The addition of MWCNT particles enhances the convective heat transfer, increases the vortices' sizes, and promotes the vertical stratification of the temperature field.
- Lower heat transfer is observed with the increasing Hartmann number and the variation of heat transfer is almost smooth. In other words, oscillation of heat transfer becomes very weak.
- For the same Hartmann number, higher heat transfer and lower amplitude are formed at a higher nanoparticle volume fraction.

Author Contributions: In this paper, L.K., H.F.O. and K.G. conceived and designed the numerical experiments. L.K. and M.A.A. performed the experiments. H.A.M., H.B. and N.A.-H. analyzed the data. H.F.O., K.G. and L.K. wrote the paper.

Conflicts of Interest: The authors declare no conflict of interest.

Nomenclature

$\vec{B}$	Magnetic field ($= \vec{B}' / B_0$)
Be	Bejan number
C_p	Specific heat at constant pressure (J/kg·K)
$\vec{E}$	Dimensionless electric field
$\vec{e}_B$	Direction of magnetic field
g	Gravitational acceleration (m/s^2)
$\vec{J}$	Dimensionless density of electrical current
k	Thermal conductivity (W/m.K)
l	Enclosure width
n	Unit vector normal to the wall
N_s	Dimensionless local generated entropy
Nu	Local Nusselt number
Pr	Prandtl number
Ra	Rayleigh number
t	Dimensionless time ($t' \cdot \alpha / l^2$)
T	Dimensionless temperature [$(T' - T'_c) / (T'_h - T'_c)$]

T'_c	Cold temperature (K)
T'_h	Hot temperature (K)
T_o	Bulk temperature [$T_o = (T'_c + T'_h)/2$]
$\vec{V}$	Dimensionless velocity vector ($\vec{V}' \cdot l/\alpha$)
x, y, z	Dimensionless Cartesian coordinates (x'/l, y'/l, z'/l)

Greek symbols

α	Thermal diffusivity (m^2/s)
β	Thermal expansion coefficient (1/K)
ρ	Density (kg/m^3)
μ	Dynamic viscosity (kg/m.s)
ν	Kinematic viscosity (m^2/s)
Φ	Dimensionless electrical potential
φ	Nanoparticle volume fraction
σ	Electrical conductivity
$\vec{\psi}$	Dimensionless vector potential ($\vec{\psi}'/\alpha$)
$\vec{w}$	Dimensionless vorticity ($\vec{w}' \cdot \alpha/l^2$)
ΔT	Dimensionless temperature difference

Subscripts

av	Average
c	Cold
h	Hot
fr	Friction
f	Fluid
n	Normal
nf	Nanofluid
s	Solid (nanoparticle)
x, y, z	Cartesian coordinates

Superscript

′	Dimensional variable

References

1. Jaafar, M.; Gomez-Herrero, J.; Gil, A.; Ares, P.; Vazquez, M.; Asenjo, A. Variable-field magnetic force microscopy. *Ultramicroscopy* **2009**, *109*, 693–699. [CrossRef] [PubMed]

2. Izadi, M.; Mohebbi, R.; Delouei, A.A.; Sajjadi, H. Natural convection of a magnetizable hybrid nanofluid inside a porous enclosure subjected to two variable magnetic fields. *Int. J. Mech. Sci.* **2019**, *151*, 154–169. [CrossRef]

3. Hatami, M.; Zhou, J.; Geng, J.; Jing, D. Variable magnetic field (VMF) effect on the heat transfer of a halfannulus cavity filled by Fe$_3$O$_4$-water nanofluid under constant heat flux. *J. Magn. Magn. Mater.* **2018**, *451*, 173–182. [CrossRef]

4. Hashim, A.; Khan, M. Unsteady mixed convective flow of Williamson nanofluid with heat transfer in the presence of variable thermal conductivity and magnetic field. *J. Mol. Liq.* **2018**, *260*, 436–446. [CrossRef]

5. Sheikholeslami, M.; Vajravelu, K. Nanofluid flow and heat transfer in a cavity with variable magnetic field. *Appl. Math. Comput.* **2017**, *298*, 272–282. [CrossRef]

6. Sandeep, N.; Animasaun, I.L. Heat transfer in wall jet flow of magnetic-nanofluids with variable magnetic field. *Alex. Eng. J.* **2017**, *56*, 263–269. [CrossRef]

7. Hatami, M.; Khazayinejad, M.; Jing, D. Forced convection of Al$_2$O$_3$–water nanofluid flow over a porous plate under the variable magnetic field effect. *Int. J. Heat Mass Transf.* **2016**, *102*, 622–630. [CrossRef]

8. Shah, R.A.; Khan, A.; Shuaib, M. On the study of flow between unsteady squeezing rotating discs with cross diffusion effects under the influence of variable magnetic field. *Heliyon* **2018**, *4*, e00925. [CrossRef]

9. Nimmagadda, R.; Haustein, H.D.; Asirvathamb, L.G.; Wongwises, S. Effect of uniform/non-uniform magnetic field and jet impingement on the hydrodynamic and heat transfer performance of nanofluids. *J. Magn. Magn. Mater.* **2019**, *479*, 268–281. [CrossRef]

10. Nassar, M.S.; Hegazi, A.A.; Mousa, M.G. Combined effect of pulsating flow and magnetic field on thermoelectric cooler performance. *Case Stud. Therm. Eng.* **2019**, *13*, 100403. [CrossRef]

11. Kefayati, G.H.R. Lattice Boltzmann simulation of MHD natural convection in a nanofluid-filled cavity with sinusoidal temperature distribution. *Powder Technol.* **2013**, *243*, 171–183. [CrossRef]

12. Al-Salem, K.; Oztop, H.F.; Pop, I.; Varol, Y. Effects of moving lid direction on MHD mixed convection in a linearly heated cavity. *Int. J. Heat Mass Transf.* **2012**, *55*, 1103–1112. [CrossRef]

13. Bao, S.R.; Zhang, R.P.; Rong, Y.; Zhi, X.Q.; Qiu, L.M. Interferometric study of the heat and mass transfer during the mixing and evaporation of liquid oxygen and nitrogen under non-uniform magnetic field. *Int. J. Heat Mass Transf.* **2019**, *136*, 10–19. [CrossRef]

14. Malvandi, A. Film boiling of magnetic nanofluids (MNFs) over a vertical plate in presence of a uniform variable-directional magnetic field. *J. Magn. Magn. Mater.* **2016**, *406*, 95–102. [CrossRef]

15. Nessab, W.; Kahalerras, H.; Fersadou, B.; Hammoudi, D. Numerical investigation of ferrofluid jet flow and convective heat transfer under the influence of magnetic sources. *Appl. Therm. Eng.* **2019**, *150*, 271–284. [CrossRef]

16. Maraj, E.N.; Shaiq, S. Instigated magnetic field effect on carbon nanotubes suspensions encompassing variable thermophysical characteristics. *J. Phys. Chem. Solids* **2019**, *132*, 145–156. [CrossRef]

17. Bhatti, M.M.; Ellahi, R.; Zeeshan, A. Study of variable magnetic field on the peristaltic flow of Jeffrey fluid in a non-uniform rectangular duct having compliant walls. *J. Mol. Liq.* **2016**, *222*, 101–108. [CrossRef]

18. Nandy, S.K.; Mahapatra, T.R.; Pop, I. Unsteady separated stagnation-point flow over a moving porous plate in the presence of a variable magnetic field. *Eur. J. Mech. B Fluids* **2015**, *53*, 229–240. [CrossRef]

19. Sheikholeslami, M.; Vajravelu, K.; Rashidi, M.M. Forced convection heat transfer in a semi annulus under the influence of a variable magnetic field. *Int. J. Heat Mass Transf.* **2016**, *92*, 339–348. [CrossRef]

20. Qin, Y.; Luo, J.; Chen, Z.; Mei, G.; Yan, L.-E. Measuring the albedo of limited-extent targets without the aid of known-albedo masks. *Sol. Energy* **2018**, *171*, 971–976. [CrossRef]

21. Al-Rashed, A.A.A.; Kalidasan, K.; Kolsi, L.; Aydi, A.; Malekshah, E.H.; Hussein, A.K.; Kanna, P.R. Three-Dimensional Investigation of the Effects of External Magnetic Field Inclination on Laminar Natural Convection Heat Transfer in CNT–Water Nanofluid Filled Cavity. *J. Mol. Liq.* **2018**, *252*, 454–468. [CrossRef]

22. Al-Rashed, A.A.A.; Kolsi, L.; Oztop, H.F.; Aydi, A.; Malekshah, E.H.; Abu-Hamdeh, N.; Borjini, M.N. 3D magneto-convective heat transfer in CNT-nanofluid filled cavity under partially active magnetic field. *Phys. E Low Dimens. Syst. Nanostruct.* **2018**, *99*, 294–303. [CrossRef]

23. Al-Rashed, A.; Kolsi, L.; Kalidasan, K.; Malekshah, E.H.; Borjini, M.N.; Kanna, P.R. Second law analysis of natural convection in a CNT-Water Nanofluid filled inclined 3D Cavity with incorporated Ahmed Body. *Int. J. Mech. Sci.* **2017**, *130*, 399–415. [CrossRef]

24. Al-Rashed, A.A.A.; Aich, W.; Kolsi, L.; Mahian, O.; Hussein, A.K.; Borjini, M.N. Effects of movable-baffle on heat transfer and entropy generation in a cavity saturated by CNT suspensions: Three dimensional modeling. *Entropy* **2017**, *19*, 200. [CrossRef]

25. Wolthers, M.H.G.; Duits, D.; van den Ende, J. Mellema. Shear history dependence of aggregated colloidal dispersions. *Rheology* **1996**, *40*, 799–811. [CrossRef]

26. Cross, M.M. Viscosity-concentration-shear rate relations for suspensions. *Rheol. Acta* **1975**, *14*, 402–403. [CrossRef]

27. Halelfadl, S.; Estellé, P.; Aladag, B.; Doner, N.; Maré, T. Viscosity of carbon nanotubes water based nanofluids: Influence of concentration and temperatureInt. *J. Sci.* **2013**, *71*, 111–117. [CrossRef]

28. Nan, C.W.; Liu, G.; Lin, Y.; Li, M. Interface effect on thermal conductivity of carbon nanotube composites. *Appl. Phys. Lett.* **2004**, *85*, 3549–3551. [CrossRef]

29. Ozoe, H.; Okada, K. The Effect of the Direction of the External Magnetic Field on the Three-Dimensional Natural Convection in a Cubical Enclosure. *Int. J. Heat Mass Transf.* **1989**, *32*, 1939–1954. [CrossRef]

30. Jahanshahi, M.; Hosseinizadeh, S.F.; Alipanah, M.; Dehghani, A.; Vakilinejad, G.R. Numerical simulation of free convection based on experimental measured conductivity in a square cavity using Water/SiO_2 nanofluid.Int. Commun. *Heat Mass Transf.* **2010**, *37*, 687–694. [CrossRef]

31. Al-Najem, N.M.; Khanafer, K.M.; El-Refaee, M.M. Numerical Study of Laminar Natural Convection in Tilted Enclosure with Transverse Magnetic Field. *Int. J. Numer. Meth. Heat Flow* **1998**, *8*, 651–672. [CrossRef]

32. Xu, B.; Li, B.Q.; Stock, E. An Experimental Study of Thermally Induced Convection of Molten Galliumin Magnetic Fields. *Int. J. Heat Mass Transf.* **2006**, *49*, 2009–2019. [CrossRef]

33. Sheikholeslami, M. New computational approach for exergy and entropy analysis of nanofluid under the impact of Lorentz force through a porous media. *Comput. Methods Appl. Mech. Eng.* **2019**, *344*, 319–333. [CrossRef]

34. Sheikholeslami, M. Numerical approach for MHD Al2O3-water nanofluid transportation inside a permeable medium using innovative computer method. *Comput. Methods Appl. Mech. Eng.* **2019**, *344*, 306–318. [CrossRef]

35. Sheikholeslami, M. Application of Darcy law for nanofluid flow in a porous cavity under the impact of Lorentz forces. *J. Mol. Liq.* **2018**, *266*, 495–503. [CrossRef]

36. Sheikholeslami, M. Finite element method for PCM solidification in existence of CuO nanoparticles. *J. Mol. Liq.* **2018**, *265*, 347–355. [CrossRef]

37. Sheikholeslami, M. Solidification of NEPCM under the effect of magnetic field in a porous thermal energy storage enclosure using CuO nanoparticles. *J. Mol. Liq.* **2018**, *263*, 303–315. [CrossRef]

38. Sheikholeslami, M.; Omid, M. Enhancement of PCM solidification using inorganic nanoparticles and an external magnetic field with application in energy storage systems. *J. Clean. Prod.* **2019**, *215*, 963–977. [CrossRef]

39. Sheikholeslami, M.; Haq, R.; Shafee, A.; Li, Z.; Elaraki, Y.G.; Tlili, I. Heat transfer simulation of heat storage unit with nanoparticles and fins through a heat exchanger. *Int. J. Heat Mass Transf.* **2019**, *135*, 470–478. [CrossRef]

40. Sheikholeslami, M.; Haq, R.; Shafee, A.; Li, Z. Heat transfer behavior of Nanoparticle enhanced PCM solidification through an enclosure with V shaped fins. *Int. J. Heat Mass Transf.* **2019**, *130*, 1322–1342. [CrossRef]

41. Sheikholeslami, M.; Shehzad, S.A.; Li, Z.; Shafee, A. Numerical modeling for Alumina nanofluid magnetohydrodynamic convective heat transfer in a permeable medium using Darcy law. *Int. J. Heat Mass Transf.* **2018**, *127*, 614–622. [CrossRef]

42. Sheikholeslami, M.; Li, Z.; Shafee, A. Lorentz forces effect on NEPCM heat transfer during solidification in a porous energy storage system. *Int. J. Heat Mass Transf.* **2018**, *127*, 665–674. [CrossRef]

43. Sheikholeslami, M.; Jafaryar, M.; Saleem, S.; Li, Z.; Shafee, A.; Jiang, Y. Nanofluid heat transfer augmentation and exergy loss inside a pipe equipped with innovative turbulators. *Int. J. Heat Mass Transf.* **2018**, *126*, 156–163. [CrossRef]

44. Sheikholeslami, M.; Ghasemi, A.; Li, Z.; Shafee, A.; Saleem, S. Influence of CuO nanoparticles on heat transfer behavior of PCM in solidification process considering radiative source term. *Int. J. Heat Mass Transf.* **2018**, *126*, 1252–1264. [CrossRef]

45. Sheikholeslami, M.; Darzi, M.; Li, Z. Experimental investigation for entropy generation and exergy loss of nano-refrigerant condensation process. *Int. J. Heat Mass Transf.* **2018**, *125*, 1087–1095. [CrossRef]

46. Sheikholeslami, M.; Shehzad, S.A.; Li, Z. Water based nanofluid free convection heat transfer in a three dimensional porous cavity with hot sphere obstacle in existence of Lorenz forces. *Int. J. Heat Mass Transf.* **2018**, *125*, 375–386. [CrossRef]

47. Sheikholeslami, M.; Jafaryar, M.; Li, Z. Nanofluid turbulent convective flow in a circular duct with helical turbulators considering CuO nanoparticles. *Int. J. Heat Mass Transf.* **2018**, *124*, 980–989. [CrossRef]

48. Sheikholeslami, M.; Ghasemi, A. Solidification heat transfer of nanofluid in existence of thermal radiation by means of FEM. *Int. J. Heat Mass Transf.* **2018**, *123*, 418–431. [CrossRef]

49. Sheikholeslami, M.; Shehzad, S.A. CVFEM simulation for nanofluid migration in a porous medium using Darcy model. *Int. J. Heat Mass Transf.* **2018**, *122*, 1264–1271. [CrossRef]

50. Sheikholeslami, M.; Seyednezhad, M. Simulation of nanofluid flow and natural convection in a porous media under the influence of electric field using CVFEM. *Int. J. Heat Mass Transf.* **2018**, *120*, 772–781. [CrossRef]

51. Sheikholeslami, M.; Rokni, H.B. Numerical simulation for impact of Coulomb force on nanofluid heat transfer in a porous enclosure in presence of thermal radiation. *Int. J. Heat Mass Transf.* **2018**, *118*, 823–831. [CrossRef]
52. Sheikholeslami, M.; Shehzad, S.A. Numerical analysis of Fe_3O_4-H_2O nanofluid flow in permeable media under the effect of external magnetic source. *Int. J. Heat Mass Transf.* **2018**, *118*, 182–192. [CrossRef]